# Recent research progress in $CO_2$ hydrate based cold thermal energy storage

**Xiaolin Wang*, Fengyuan Zhang and Wojciech Lipiński**

Research School of Electrical, Energy and Materials Engineering, The Australian National University, Canberra, ACT 2601, Australia

**Abstract**

Carbon dioxide ($CO_2$) gas hydrates based cold thermal energy storage is an emerging promising technology for applications in residential, commercial and service building air conditioning. The main research topics include experimental and theoretical methods to study $CO_2$ hydrate thermodynamics and kinetics, lab-scale cold storage system demonstration, and system modelling and integration, which have rarely been intensively reviewed. This paper reviews of the state of the art as well as potential future research directions in the field. Numerous discussion points are based on authors' own work.

*Keywords: $CO_2$ gas hydrate, cold thermal energy storage, thermodynamics, kinetics*

## 1. Introduction

Cold thermal energy storage (CTES) is suited to air conditioning (AC) systems in residential, commercial and service buildings including schools, hospitals, data centres and hotels. A typical configuration of an AC system with CTES is shown in Figure 1. In this way, cooling can be produced at opportune times and later deployed for cooling service. The use of CTES with air conditioners provides a number of cost and efficiency advantages including (*i*) lower electricity bills by accessing off-peak electricity rates, (*ii*) lower peak electricity charges and demand-side management requirements, (*iii*) increased chiller efficiency through night operation and reduced chiller start cycles, (*iv*) increased chiller efficiency by load sharing with CTES, (*v*) reduced chiller size and initial cost, and (*vi*) CTES is cheaper than electrical batteries.

Commercially used cold storage media include water, ice and phase change materials (PCMs). The inherent challenges associated with the use of those media have prevented them from broad deployment. Chilled water has a very low energy storage density that causes the cold storage to take up a large volume. Storing ice requires a dedicated glycol chiller which is expensive and has low energy efficiency. Conventional PCMs are normally expensive and may exhibit chemical instability and phase segregation [Zhai et al. 2013; Sarbu and Sebarchievici, 2018].

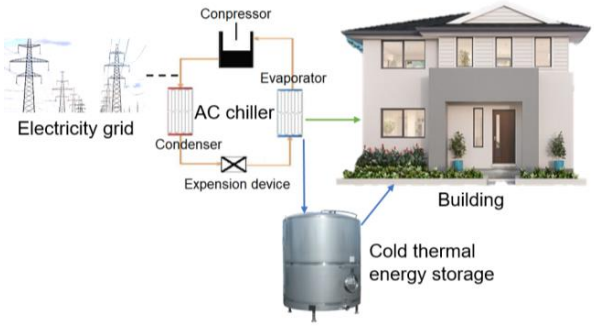


**Fig. 1: Configuration of cold thermal storage in an AC system**

**Fig. 2: $CO_2$ hydrate formed in a pressure vessel (Wang 2016b)**

Gas hydrates are ice-like compounds consisting of water molecules forming a clathrate structure to host guest gas molecules. The guest gas is typically hydrogen ($H_2$), nitrogen ($N_2$), carbon dioxide ($CO_2$), methane ($CH_4$), ethane ($C_2H_6$), propane ($C_3H_8$), or mixtures of thereof, for example in form of natural gas. Applications include CTES, hydrate-based carbon capture and sequestration (Lee et al. 2017a; Lee et al. 2018; Lee et al. 2017b; Xia et al. 2017; Xu et al. 2019), gas separation (Azimi and Mirzaei 2016; Chen et al. 2017; Horii and Ohmura 2018; Liu et al. 2018) including biogas upgrading




doi:10.18086/swc.2019.24.10 Available at http://proceedings.ises.org

(Castellani et al. 2017; Yue et al. 2018), hydrate-based desalination (Babu et al. 2018; Croeser et al. 2019), separation processes in food processing (Li et al. 2015), intesification of algal biomass production (Nakano et al. 2014), transportable cooling carriers (Youssef et al. 2019), and environmentally friendly refrigeration (Kim et al. 2017a; Wang et al. 2014).

$CO_2$ hydrates have characteristics that enable them as promising cold storage media, including suitable phase equilibrium temperature range for AC applications (adjustable in the 0–14ºC temperature range (Wang and Dennis 2016a; Wang and Dennis 2017b), high latent heat (501–507 kJ $kg^{-1}$ for pure $CO_2$ hydrates (Fournaison et al. 2004); 318–441 kJ $kg^{-1}$ for $CO_2$ hydrate with various promoters (Kim et al. 2017a; Wang and Dennis 2016a; Wang and Dennis 2017b)), low material cost, and chemical safety (Wang et al. 2014). The appearance of $CO_2$ hydrate crystals formed in a pressure vessel is shown in Figure 2 (Wang 2016b). The thermal storage process is realised through exothermic hydrate formation (equation (1)) and endothermic hydrate dissociation (equation (2)):

$$CO_2 + nH_2O \rightarrow CO_2 \cdot nH_2O + \text{heat} \quad (1)$$

$$CO_2 \cdot nH_2O + \text{heat} \rightarrow CO_2 + nH_2O \quad (2)$$

In the last decade, there have been a large number of studies on $CO_2$ hydrate material fundamental research and proof-of-concept trials of $CO_2$ hydrate based CTES systems. Many studies focused on improving equilibrium conditions and thermal properties of $CO_2$ hydrate in order to enhance its viability in thermal storage applications. There is a lack of reviews that summarise fundamental studies on $CO_2$ gas hydrate formation thermodynamics and kinetics as well as its CTES application in system demonstrations. This paper provides a comprehensive review on these significant topics and focuses on newly published articles.

## 2. $CO_2$ hydrate equilibrium characterization

To study $CO_2$ hydrate thermodynamic and kinetic performance, various reactors (a.k.a. cells or crystallisers) have been designed to accommodate gas hydrate formation and dissociation under controlled pressure-temperature conditions with proper promoters, agitations, magnetic and/or ultrasonic fields. The design and configuration of systems are listed in Table 1. There are similarities among these reactors. Most are small-scale (<600 mL) high-pressure vessels since handling safely with high pressure in a large scale is difficult. They are mostly cylindrical, which is for a uniform radial heat transfer and/or effective stirring motion of impeller. There is a closed external cooling loop that circulates heat transfer fluid at a constant temperature to trigger gas hydrate formation. A gas cylinder is connected to the vessel with controlled pressure.

There are some common aspects in most of the designed setups and procedures that require improvements.

1) The methods to determine the start and completion of gas hydrate formation/dissociation differ among studies. Some rely on the observation of crystals to recognise the onset point of hydrate formation, while others use temperature and pressure curves, i.e. taking the inflection point in the curve or derivative curve of temperature or pressure (indicates the highest changing rate) as the point when hydrate formation and dissociation take place. These methods should be unified as it is less convincing to compare data generated from different methods.

2) The mass of sample, size and material of the reactor and cooling/heating rate are all found to affect the measurement result and its accuracy. In order to reduce the effect of heat transfer rate, stepwise cooling and heating are applied in most cases to determine the phase equilibrium.

3) Heat transfer and mass transfer during gas hydrate formation is usually restricted by the experimental setup, especially when the liquid in reactor is stationary. When cooling is proceeded, gas hydrates tend to first form on cooling surfaces, since the low surface temperature provides nucleation driving force and the surface roughness provides nucleation sites. However, the formed hydrates cause resistance of heat and mass transfer, which leads to slow and incomplete gas hydrate formation in experiments and in turn reduces the accuracy of results.

In addition to tradition thermodynamics and kinetics studies, there are novel approaches proposed for efficient $CO_2$ hydrate formation and accurate nucleation observation. By Ambuehl et al. (Ambuehl and Elwood Madden 2014), $CO_2$ infused ice experiments were proposed. In order to test the effects of $CO_2$ within ice on hydrate formation, ultrapure water was infused with $CO_2$ gas and frozen prior to the hydrate formation, which allowed much of the gas to exsolve. $CO_2$ consumption and release rates both increased significantly in infused ice experiments. $CO_2$ bubbles formed during the freezing of the infused ice likely provided larger surface area for hydrate nucleation, increasing the rate of formation. Atig et al. (Atig et al. 2018)

designed a droplet-based millifluidic method for investigating hydrate nucleation and growth, which consisted of a transparent capillary and a train of regularly-spaced droplets of an aqueous phase in a carrier oil. The nucleation and growth were video-monitored as temperature and pressure were suited. The novelty of this approach is the ability to work under pressure with dissolved gas, which opens the way to investigations of gas hydrate nucleation in addition to ice nucleation.

## 3. Thermodynamic and kinetic modelling of $CO_2$ hydrate formation and dissociation

Most widely-used models are thermodynamic models and kinetic models with the former related with the driving force while the latter made for equilibria calculation (Sun and Kang 2016).

The thermodynamic model is based on the basic statistic thermodynamic models derived by Van der Waals and Platteeuw (vdW–P) with Leonard–Jones potential function to calculate gas hydrate dissociation pressure. Cage occupancies of a $CO_2$ + $CH_4$ system were predicted based on the vdW–P thermodynamic theory with the Langmuir adsorption model and Peng–Robinson question of state. In the work of Sadeq et al., results indicated that the model was accurate at pressures <10 MPa, while it had considerable deviation at more extreme pressures where $CO_2$ had a propensity to occupy the large cavities of sI cages (Sadeq et al. 2017). By Waseem et al. (Waseem and Alsaifi 2018), a thermodynamic modelling approach was built to predict gas hydrate formation conditions based on vdW–P model for hydrate phase and SAFT–VR Mie equation of state (EOS) for vapour and liquid phases. Three different association schemes into the SAFT–VR Mie EOS were employed to account for hydrogen bonds between water molecules, namely square-well, Lennard–Jones and Mie potentials. The results compared with experimental data showed excellent predictions of dissociation pressures for single and mixed gases without readjustment of the Langmuir constants. By Herslund et al. (Herslund et al. 2014a), a thermodynamic model, based on vdW–P model and Cubic-Plus-Association (CPA) EOS was applied to model mixed-promoter systems of single and binary $CO_2$-rich mixtures containing $N_2$, $CH_4$, $C_2H_6$, $C_3H_8$, isobutene, hydrogen sulfide and methanol for temperatures above 180 K and pressures below 100 MPa. The model explained the synergistic effect by the fact that THF displaces cyclopentane (CP) from the large cavities of sII hydrate. The largest pressure reduction effect was predicted where approx. half of the CP in the hydrate phase was substituted with THF. A simplified EOS based on hydrogen bonding non-random lattice fluid theory was applied for both vapour and liquid phases. The two-phase and three-phase equilibrium calculations were found to be comparable with another study and better for water contents in liquid $CO_2$ in equilibrium with gas hydrates (Lee et al. 2016). A thermodynamic model based on the CPA EOS and the vdW–P hydrate model was applied by Herslund et al. (Herslund et al. 2014b) to perform an evaluation of gas hydrate systems. In order to reduce the entropy generation rate in gas hydrate dissociation, the entropy generation minimisation was set as the objective to perform an thermodynamic optimisation for gas hydrate dissociation (Bi et al. 2016). By establishing thermodynamic optimization model, both the optimal control strategy and the optimal heating rate of gas hydrate dissolution process were determined. The entropy generation rate related to the optimal heating rate decreased by 7.5% compared with normal situation. The research results provided guidelines for optimal design of gas hydrate based CTES systems.

In kinetic modelling, main driving forces, such as chemical potential difference, mole fraction of $CO_2$ dissolved difference, fugacity difference, subcooling degree, and Gibbs free energy difference, are analysed. In the work of Khosharay et al. (Khosharay et al. 2015), the formation kinetics of $CH_4$ and $CO_2$ hydrates was studied. A kinetic model based on the mass transfer restriction of the gas through the liquid film was used to describe the kinetics of gas hydrate formation. Besides, in order to determine interfacial mole fraction of hydrate former, a Parachor model for interfacial properties was employed. A semi-empirical kinetic model presented by Rasoolzadeh et al. (Rasoolzadeh et al. 2016) was used in the work of Moeini et al (Moeini et al. 2018). Results showed that the proposed model was able to predict the induction time of $CO_2$ hydrate formation with a good accuracy. A chemical affinity model was used for modelling of hydrate formation kinetics, and its parameters were obtained for one-stage and two-stage kinetics. The results showed that the model was successful for the kinetics of $CO_2$ + THF hydrate formation prediction (Roosta et al. 2015).

**Tab. 1: $CO_2$ hydrate characterizing reactor structure and system configuration**

| Gas composition | Promoters | Properties characterised | Key method | Main component | Operating conditions | Scale | Agitation | Main findings and accuracy | Ref. |
|---|---|---|---|---|---|---|---|---|---|
| $CO_2$ | TBAB, TBAF, SDS, $TiO_2$ nanoparticle | Equilibrium, enthalpy, $CO_2$ consumption, induction time, supercooling degree | T-history method | High-pressure horizontal reaction tube | 279.0–288.0 K, 0.1–1 MPa | 10-mm internal diameter and 160-mm length | Not used | • Hydrate formula was $2.49CO_2 \cdot TBAB \cdot 38H_2O$, and the hydrate formation enthalpy was 318.5 J $g^{-1}$ (hydrate).<br>• This result was in agreement with literature. | Wang et al. 2016a |
| $CH_4$ and $CO_2$ | Not used | Three-phase equilibrium, gas solubility in aqueous phases | Isochoric pressure-search method, phase boundary dissociation method | High-pressure pressure-volume-temperature (PVT) cell in an air bath | 278.6–283.4 K, 2.33–9.68 MPa | 325 ml | Magnet stirrer | • Data were compared against reported experimental data in literature and very good agreement was achieved for both systems. | Kastanidis et al. 2016 |
| $CO_2$ (0.148/0.395/0.750 mol%) + $H_2$ (0.852/0.605/0.250 mol%) | TBAB (0.05, 0.30 wt%) | Three-phase equilibrium | Isochoric pressure-search method | High-pressure equilibrium cell | 275.5–292.8 K, up to 15.9 MPa | 201.5-$cm^3$ internal volume | Motor-driven turbine agitation | • Significant decrease in operating pressure of gas hydrate formation from the corresponding gas mixtures was observed due to the promotion of TBAB. | Mohammadi et al. 2013 |
| $CO_2$ | THF, CP, mixture of THF+CP | Dissociation conditions | Isochoric temperature-search method | Equilibrium cell consists of a jacketed crystalliser with temperature controlled | 282.4–293.2 K, 0.42–3.70 MPa | 66.5-ml internal volume | Magnetic stirrer | • Dissociation pressures by adding THF was lower than those of CP promoted system. By adding 5 mol% THF to the CP promoted system, hydrate dissociation pressures were reduced by 20%. | Herslund et al. 2014a |
| $CO_2$ (0.151/0.399/0.749 mol%) + $N_2$ (0.849/0.601/0.251 mol%) | TBAB (0.05, 0.30 wt%) | Phase equilibrium | Isochoric method combined with gas phase sampling technique | High-pressure cell in a temperature-controlled bath with a gas chromatography (GC) | 275.2–289.2 K, 0.581–19.1 MPa | 201.1-$cm^3$ internal volume including transfer lines | Stirrer at constant speed of 1500 rpm | • Significant change of $CO_2$ concentration in the gas phase was observed under hydrate stability conditions. | Belandria et al. 2012 |
| $CH_4$ and $CO_2$ | Not used | Gas hydrate formation kinetics | Isochoric pressure-search method | Autoclave | 276.0 K, 0–3.5 MPa | 430-ml internal volume | Magnet stirrer at 0–1400 rpm | • Formation was accelerated by better mixing, higher supersaturation and memory effect. | He et al. 2011 |

| Gas composition | Promoters | Properties characterised | Key method | Main component | Operating conditions | Scale | Agitation | Main findings and accuracy | Ref. |
|---|---|---|---|---|---|---|---|---|---|
| $CO_2$ | Not used | $CO_2$ hydrate formation as a function of rotation speed, temperatures, and initial pressures | Isochoric pressure-search method | Cylindrical high-pressure reactor with impeller to induce gas through an orifice in the hollow shaft above the liquid surface | 274.2–279.2 K, 2.09–6.02 MPa | 300-ml maximum volume of gas enclosed | Gas-inducing impeller at up to 800 rpm | • $CO_2$ hydrate formation was efficiently enhanced by mechanical agitation and gas recycle.<br>• The induction time was shortened from 261 to 24 min as increasing agitation speed.<br>• Reactor, temperature and initial pressure all significantly affected $CO_2$ hydrate formation. | Li et al. 2017 |
| $CO_2$ | THF (3 mol%), SDS (0–2000 mg $L^{-1}$), porous media | The effects of a mixture of additives, on $CO_2$ hydrate formation | A graphic method, the Gibbs phase rule | High pressure vessel | 279.3–291.6 K, 0.22–4.65 MPa | 476 ml | Not used | • Shortest induction time was at 1000 mg $L^{-1}$ SDS, but a small decrease in the final hydrate saturation was at 1000 mg $L^{-1}$ SDS. | Yang et al. 2013 |
| $CO_2 + CH_4$, $N_2 + CH_4$, $CO_2 + N_2$ | Not used | Dissociation conditions | Isochoric temperature-search method | Cryogenic sapphire cell | 275.8–294.0 K, 5–25 MPa | 60-ml internal volume | Electric stirrer at 550 rpm | • The statistical analysis of the obtained data showed a maximum experimental error of 1.65%. | Sadeq et al. 2017 |
| $CO_2$ (15.1%) + $N_2$ (84.9%), $CO_2$ (39.9%) + $N_2$ (60.1%) | TBAB (0.05, 0.15, 0.30 wt%) | Dissociation conditions | Isochoric pressure-search method | Hastelloy cylindrical vessel | 277.1–293.2 K<br>16.2 MPa | 30 $cm^3$ | Magnetic stirrer | • The measured phase equilibrium data demonstrated high hydrate promotion effects of TBAB aqueous solutions. | Mohammadi et al. 2012 |
| $CO_2$ (40%) + $H_2$ (60%) | TBAB (0.29 mol%) | Morphology and hydrate kinetics | Isochoric method | Stainless steel reactor with GC | 275.2–277.2 K, 1.5–5.5 MPa | 100 mL | Not used | • TBAB hydrate formation and TBAB–gas mixture hydrate formation were two independent processes.<br>• $CO_2$ recovery under static conditions had been greatly improved compared to the stirring process. | Yu et al. 2018 |
| $CO_2 + H_2$ | TBAB (0.14–2.67 mol%) | Phase equilibrium | Compositional analysis and resistance detecting method | High-pressure stainless steel hydrate crystalliser | 274.1–288.6 K, 0.25–7.26 MPa | 336 $cm^3$ | Magnetic stirrer | • The hydrate formation pressure of the $CO_2 + H_2$ + TBAB mixture was remarkably lower than that of $CO_2 + H_2$ mixture at the same temperature, and decreased with the increase in TBAB concentration. | Li et al. 2010 |

| Gas composition | Promoters | Properties characterised | Key method | Main component | Operating conditions | Scale | Agitation | Main findings and accuracy | Ref. |
|---|---|---|---|---|---|---|---|---|---|
| $CO_2$ | Not used | Fugacity or solubility as a driving force in formation, effect of temperature and pressure on gas solubility | Isochoric pressure-search method | Crystallizer and auxiliary cell with an insulated bath | 275.2 and 281.2 K, 1.85–3.97 MPa | 271 $cm^3$ | Magnetic stirrer at 270 rpm | • Solubility of $CO_2$ in water during hydrate growth is time-independent. | Najafi et al. 2014 |
| $CO_2$ | THF | Hydrate formation kinetics | Isochoric pressure-search method | Cylindrical high-pressure reactor with a thermostatic bath and a controllable circulator | 275.2–284.2 K, 2.09–2.66 MPa | 600 $cm^3$ | Four-blade mixer at 800 rpm | • The chemical affinity model is suitable for the kinetics of $CO_2$ + THF hydrate. | Roosta et al. 2015 |
| $CO_2$ | SDS, lauryl alcohol ethoxylate (LAE), lauryl alcohol ethoxylate-2 (LAE2) | Hydrate formation kinetics in order to maximise the heat flow rate | Thermal analysis | Two high-pressure cells | 258.0–288.0 K, up to 20 MPa | Approx. 1 $cm^3$ | Not used | • LAE2 led to a larger increase in the kinetics.<br>• The optimal values of $CO_2$ hydrate formation was at 3.045 MPa with LAE2 at 29 ppm. | Naeiji et al. 2018 |
| $CO_2$-rich gas | Not used | Three-phase equilibrium, quadruple point | Isochoric pressure-search method | A stainless steel cylindrical vessel | 269.6–275.8 K, 0.825–1.71 MPa | 200-$cm^3$ internal volume | Magnetic impeller | • The determined p–T condition at quadruple point was 271.6 ± 0.2 K and 1.04 ± 0.02 MPa.<br>• The equilibrium data obtained are in agreement with the literature data. | Nema et al. 2017 |
| $CO_2$ | Not used | The effect of initial pressure, temperature, flowrate, and liquid loading on $CO_2$ hydrate formation | $CO_2$ injection in flow loop with cold glycol with the desired temperature | Flow loop with flowrate between 16–48 L $min^{-1}$ and liquid loadings 66.7, 73.3, 80.0 vol% | 274.2–277.2 K, 4.5–6.5 MPa | 7.5 L | Not used | • Gas consumption increased as the initial pressure increased while it decreased with the increase of the temperature, flowrate, and liquid loading. | Zhou et al. 2018 |

## 4. Lab demonstration of $CO_2$ hydrate based CTES systems

Although many have been done on the fundamental study of $CO_2$ hydrates for its suitability in CTES, only a limited number of lab demonstrations of $CO_2$ hydrate based CTES application in a cooling system has been found. By Wang et al. (Wang and Dennis 2017a, c), a lab demonstration of $CO_2$–TBAB hydrate based CTES was built in an emulated AC system, as shown in Figure 3. It was found $CO_2$ hydrate formation only proceeded when the liquid was circulated. An experimental demonstration for a shell-and-tube fluidised bed heat exchanger, combined with a $CO_2$ hydrate slurry CTES, were carried out (Zhou et al. 2015), as shown in Figure 4. Heat was removed from the CTES by circulating the slurry through a heat exchanger which was a part of the cooling distribution system. The COP of the system composed of fluidised bed for hydrate generation and storage appeared to be 23–43% higher than the COP of a conventional system. The heat transfer coefficient during hydrate generation in the fluidised bed heat exchanger was around 5000 W $m^{-2}K^{-1}$. During the operation with continuous hydrate slurry removal, solid concentrations up to 35% was maintained in the system. The influence of pressure on gas hydrates based CTES was studied using a stirred tank reactor equipped with a cooling jacket (Dufour et al. 2017; Dufour et al. 2019), shown in Figure 5. Under the same conditions and during the same charging time, the amount of stored energy using $CO_2$ hydrates can be three times higher than that using water. By increasing the initial pressure from 2.45 to 3.2 MPa at 282.15 K, it was also possible to decrease the charging time by a factor of 3. Lifting pressure to increase $CO_2$ hydrate phase change temperature improved system efficiency as it could decrease the thermal loss. Result also showed that the use of $CO_2$ hydrate slurries had beneficial impact on the heat exchanger efficiency and pressure drops under appropriate conditions. For example, $CO_2$ hydrate slurry at 25 kg $h^{-1}$ and 8% hydrate mass fraction presented half the pressure drop of water at 100 kg $h^{-1}$ with higher heat exchange. A small-scale gas hydrate CTES apparatus was designed (Xie et al. 2010), shown in Figure 6. The cooling capacity, growth rate, hydrate packed factor and overall heat transfer coefficient were calculated under different heat exchangers, SDS additive concentrations, cooling fluid temperatures and flowrates. Results showed that the performance could be improved greatly by adding a heat exchanger with vertical metal fins and using SDS with concentration of 0.04 wt%. Decreasing cooling fluid temperature or increasing its flowrate also increased the cooling storage capacity. In addition, a mechanical blending for 5 min was a better hydration enhancement method, which presented the perspective for practical application.

## 5. System modelling of $CO_2$ hydrate-based CTES–secondary refrigerant system

The potential presence of $CO_2$ gas hydrate in a secondary refrigeration process with CTES is a new feature, and a number of system modelling have been conducted on this process. Two types of gas hydrates were used in secondary refrigeration processes: single $CO_2$ hydrate and mixed $CO_2$–TBPB hydrate (Youssef et al. 2019). For each user, the slurry is circulated across a heat exchanger where the hydrate melts. When leaving the heat exchanger, the three-phase flow (slurry plus gas released from hydrate) enters a cyclone where centrifugal forces and gravity separates the solid–liquid slurry from $CO_2$ gas. Then the slurry returns to the secondary loop where it flows toward the next users, and eventually to storage together with $CO_2$ gas from a separated loop. The results showed that the process saved up to 75% of the total storage volume. The marginal COP of this extra cold production was up to 6. A simulated cooling system based on $CO_2$+THF hydrate was proposed (Kim et al. 2017b). $CO_2$+THF hydrate is formed at a formation reactor (1.0 °C, 1.5 MPa) by waste cooling and then transported to a dissociation reactor (6.0°C, 0.1 MPa). The chilled water of 15.0°C from the demand side enters the dissociation reactor and leaves it at a temperature of 7.0°C, cooled by the dissociation energy of the $CO_2$+THF hydrate. The dissociated $CO_2$ gas is compressed in the compressor to return to the formation reactor, and dissociated THF solution is pumped to the formation reactor. The system provides the cooling capacity of 51,600 RT for the district cooling region. Based on this, a two-stage liquefied natural gas (LNG) cooling recovery system is proposed (Choi et al. 2019). The first stage is a $NH_3/H_2O$ absorption system for cooling recovery under low temperature conditions; the second stage is a $CO_2$ hydrate CTES system harvesting cooling from −3°C of nature gas. By using hydrate slurry as the secondary refrigerant, much smaller flowrate is required compared to conventional district cooling systems. In the cases of the THF concentrations at 1.0, 1.5 and 5.56 mol%, the corresponding COPs are 12.04, 11.55 and 6.72, respectively. The COP of $CO_2$–THF hydrate slurry district cooling system for 5000 RT is higher (14.3) (Sun et al. 2017). Through a life-cycle cost analysis, the $CO_2$ hydrate system can save the energy cost by approx. $ 666,553 compared to sensible heat methods (Choi et al. 2015).

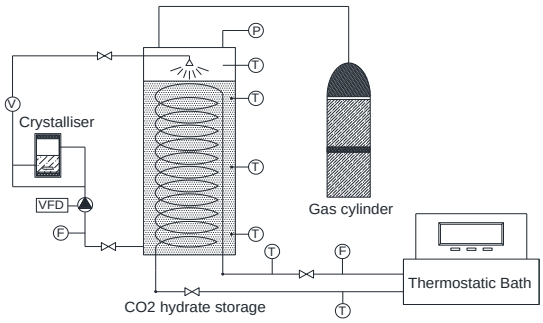


**Fig. 3: Schematic diagram of the lab-scale $CO_2$ hydrate cold storage system (Wang and Dennis 2017a, c)**

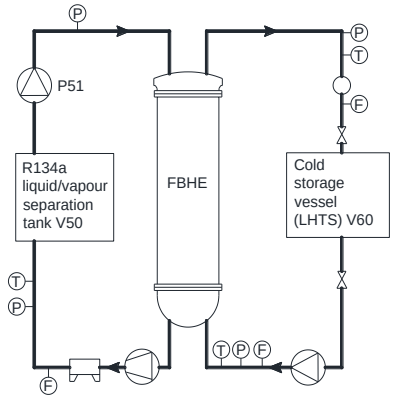


**Fig. 4: System of shell-and-tube fluidised bed heat exchanger with a $CO_2$ hydrate slurry CTES (Zhou et al. 2015)**

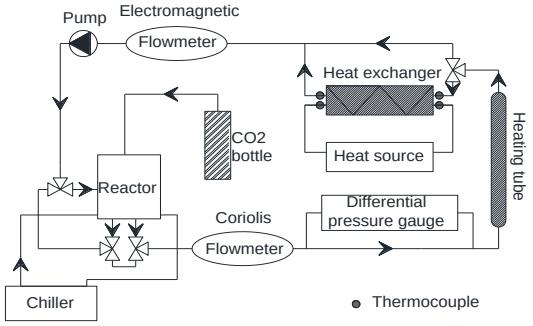


**Fig. 5: Configuration of a stirred tank reactor equipped with a cooling jacket (Dufour et al. 2017; Dufour et al. 2019)**

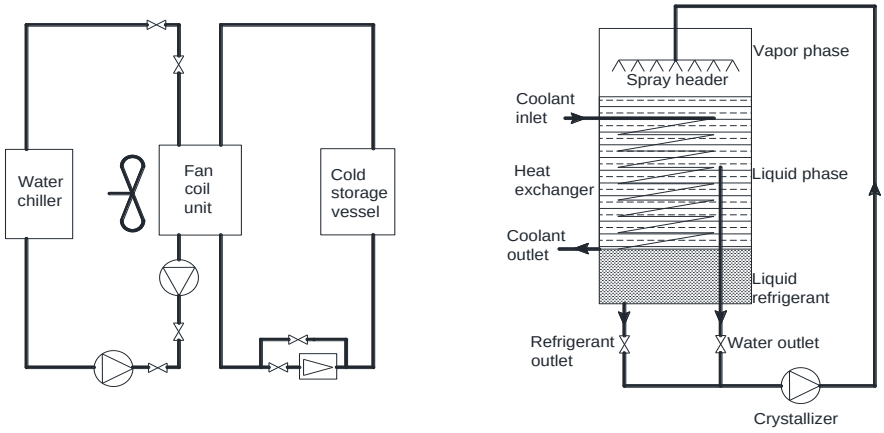


**(a) General system diagram** **(b) Diagram of CTES vessel**

**Fig. 6: Configuration of a small-scale gas hydrate CTES apparatus (Xie et al. 2010)**

## 6. Conclusions

This review has summarised the recent research progress in $CO_2$ hydrate technology for cold thermal energy storage applications, especially its thermodynamics and kinetics characterisation and enhancement. It discussed major progresses in this area including experimental and theoretical methods to study $CO_2$ hydrate thermodynamics and kinetics, lab-scale cold storage system demonstration, and system modelling and integration, which have rarely been intensively reviewed. It also summarised aspects in most of the current setups and procedures that require improvements, and suggests possible future research directions based on the authors' own work.

## References

Ambuehl, D. and Elwood Madden, M. 2014. $CO_2$ hydrate formation and dissociation rates: Application to Mars. *Icarus* 234, pp. 45-52.
Atig, D. et al. 2018. A droplet-based millifluidic method for studying ice and gas hydrate nucleation. *Chemical Engineering Science* 192, pp. 1189-1197.
Azimi, A. and Mirzaei, M. 2016. Experimental evaluation and thermodynamic modeling of hydrate selectivity in separation of $CO_2$ and $CH_4$. *Chemical Engineering Research and Design* 111, pp. 262-268.
Babu, P. et al. 2018. A review of clathrate hydrate based desalination to strengthen energy–water nexus. *ACS Sustainable Chemistry & Engineering* 6(7), pp. 8093-8107.
Belandria, V. et al. 2012. Compositional analysis of the gas phase for the $CO_2$+ $N_2$+ tetra-n-butylammonium bromide aqueous solution systems under hydrate stability conditions. *Chemical engineering science* 84, pp. 40-47.
Bi, Y. et al. 2016. Thermodynamic optimization for dissociation process of gas hydrates. *Energy* 106, pp. 270-276.
Castellani, B. et al. 2017. Experimental investigation and energy considerations on hydrate-based biogas upgrading with CO 2 valorization. *Biomass and Bioenergy* 105, pp. 364-372.
Chen, Z.-Y. et al. 2017. Carbon dioxide and sulfur dioxide capture from flue gas by gas hydrate based process. *Energy Procedia* 142, pp. 3454-3459.
Choi, J. W. et al. 2015. $CO_2$ hydrate cooling system and LCC analysis for energy transportation application. *Applied Thermal Engineering* 91, pp. 11-18.
Choi, S. et al. 2019. Experimental investigation on $CO_2$ hydrate formation/dissociation for cold thermal energy harvest and transportation applications. *Applied Energy* 242, pp. 1358-1368.
Croeser, N. et al. 2019. Investigation into the use of gas hydrate technology for the treatment of vinasse. *Fluid Phase Equilibria* 492, pp. 67-77.
Dufour, T. et al. 2017. Impact of pressure on the dynamic behavior of $CO_2$ hydrate slurry in a stirred tank reactor applied to cold thermal energy storage. *Applied Energy* 204, pp. 641-652.
Dufour, T. et al. 2019. Experimental and modelling study of energy efficiency of $CO_2$ hydrate slurry in a coil heat exchanger. *Applied Energy* 242, pp. 492-505.
Fournaison, L. et al. 2004. $CO_2$ Hydrates in Refrigeration Processes. *Industrial & Engineering Chemistry Research* 43(20), pp. 6521-6526.
He, Y. et al. 2011. Kinetics of $CO_2$ and methane hydrate formation: An experimental analysis in the bulk phase. *Fuel* 90(1), pp. 272-279.
Herslund, P. J. et al. 2014a. Measuring and modelling of the combined thermodynamic promoting effect of tetrahydrofuran and cyclopentane on carbon dioxide hydrates. *Fluid Phase Equilibria* 381, pp. 20-27.
Herslund, P. J. et al. 2014b. Modelling of cyclopentane promoted gas hydrate systems for carbon dioxide capture processes. *Fluid Phase Equilibria* 375, pp. 89-103.
Horii, S. and Ohmura, R. 2018. Continuous separation of $CO_2$ from a $H_2 + CO_2$ gas mixture using clathrate hydrate. *Applied Energy* 225, pp. 78-84.
Kastanidis, P. et al. 2016. Development of a novel experimental apparatus for hydrate equilibrium measurements. *Fluid Phase Equilibria* 424, pp. 152-161.
Khosharay, S. et al. 2015. Investigation on the kinetics of methane and carbon dioxide hydrates by using a modified kinetic model. *Journal of Natural Gas Science and Engineering* 26, pp. 587-594.
Kim, S. et al. 2017a. Characteristics of $CO_2$ hydrate formation/dissociation in $H_2O$ + THF aqueous solution and estimation of $CO_2$ emission reduction by district cooling application. *Energy* 120, pp. 362-373.
Kim, S. et al. 2017b. Characteristics of $CO_2$ hydrate formation/dissociation in $H_2O$+ THF aqueous solution and estimation of $CO_2$ emission reduction by district cooling application. *Energy* 120, pp. 362-373.
Lee, D. et al. 2017a. Guest enclathration and structural transition in CO 2 + N 2 + methylcyclopentane hydrates and their significance for CO 2 capture and sequestration. *Chemical Engineering Journal* 320, pp. 43-49.
Lee, J. H. et al. 2016. Modeling gas hydrate-containing phase equilibria for carbon dioxide-rich mixtures using an equation of state. *Fluid Phase Equilibria* 409, pp. 136-149.
Lee, Y. et al. 2018. Structural transition induced by cage-dependent guest exchange in $CH_4 + C_3H_8$ hydrates with $CO_2$ injection for energy recovery and $CO_2$ sequestration. *Applied Energy* 228, pp. 229-239.
Lee, Y. et al. 2017b. $CH_4$-$CO_2$ replacement occurring in sII natural gas hydrates for $CH_4$ recovery and $CO_2$ sequestration. *Energy Conversion and Management* 150, pp. 356-364.
Li, A. et al. 2017. An experimental study on carbon dioxide hydrate formation using a gas-inducing agitated reactor. *Energy* 134, pp. 629-637.
Li, S. et al. 2015. Concentrating orange juice through $CO_2$ clathrate hydrate technology. *Chemical Engineering Research and Design* 93, pp. 773-778.
Li, X.-S. et al. 2010. Gas Hydrate Formation Process for Capture of Carbon Dioxide from Fuel Gas Mixture. *Industrial & Engineering Chemistry Research* 49(22), pp. 11614-11619.
Liu, J. et al. 2018. Experimental study on hydrate-based gas separation of mixed $CH_4$/$CO_2$ using unstable ice in a silica gel bed. *Energy* 157, pp. 54-64.

Moeini, H. et al. 2018. Experimental study of sodium chloride aqueous solution effect on the kinetic parameters of carbon dioxide hydrate formation in the presence/absence of magnetic field. *Journal of Natural Gas Science and Engineering* 50, pp. 231-239.
Mohammadi, A. H. et al. 2012. Phase equilibrium measurements for semi-clathrate hydrates of the ($CO_2$+ $N_2$+ tetra-n-butylammonium bromide) aqueous solution system. *The Journal of Chemical Thermodynamics* 46, pp. 57-61.
Mohammadi, A. H. et al. 2013. Semi-clathrate hydrate phase equilibrium measurements for the $CO_2$+ $H_2$/$CH_4$+ tetra-n-butylammonium bromide aqueous solution system. *Chemical Engineering Science* 94, pp. 284-290.
Naeiji, P. and Varaminian, F. 2018. Kinetic study of carbon dioxide hydrate formation by thermal analysis in the presence of two surfactants: Sodium dodecyl sulfate (SDS) and lauryl alcohol ethoxylate (LAE). *Journal of Molecular Liquids* 254, pp. 120-129.
Najafi, M. and Mohebbi, V. 2014. Solubility measurement of carbon dioxide in water in the presence of gas hydrate. *Journal of Natural Gas Science and Engineering* 21, pp. 738-745.
Nakano, S. et al. 2014. A usage of $CO_2$ hydrate: convenient method to increase $CO_2$ concentration in culturing algae. *Bioresour Technol* 172, pp. 444-448.
Nema, Y. et al. 2017. Quadruple point determination in carbon dioxide hydrate forming system. *Fluid Phase Equilibria* 441, pp. 49-53.
Rasoolzadeh, A. et al. 2016. Experimental study and modeling of methane hydrate formation induction time in the presence of ionic liquids. *Journal of Molecular Liquids* 221, pp. 149-155.
Roosta, H. et al. 2015. Experimental and modeling investigation on mixed carbon dioxide–tetrahydrofuran hydrate formation kinetics in isothermal and isochoric systems. *Journal of Molecular Liquids* 211, pp. 411-416.
Sadeq, D. et al. 2017. Experimental determination of hydrate phase equilibrium for different gas mixtures containing methane, carbon dioxide and nitrogen with motor current measurements. *Journal of Natural Gas Science and Engineering* 38, pp. 59-73.
Sun, Q. and Kang, Y. T. 2016. Review on $CO_2$ hydrate formation/dissociation and its cold energy application. *Renewable and Sustainable Energy Reviews* 62, pp. 478-494.
Sun, Q. et al. 2017. Study on dissociation characteristics of $CO_2$ hydrate with THF for cooling application. *Applied Energy* 190, pp. 249-256.
Wang, X. et al. 2014. Clathrate hydrate technology for cold storage in air conditioning systems. *Renewable and Sustainable Energy Reviews* 36, pp. 34-51.
Wang, X. and Dennis, M. 2016a. Phase equilibrium and formation behaviour of $CO_2$-TBAB semi-clathrate hydrate at low pressures for cold storage air conditioning applications. *Chemical Engineering Science* 155, pp. 294-305.
Wang, X. 2016b. Carbon dioxide semi-clathrate hydrate for cold storage based air conditioning systems: materials and applications (Doctoral dissertation).
Wang, X. and Dennis, M. 2017a. Charging performance of a $CO_2$ semi-clathrate hydrate based PCM in a lab-scale cold storage system. *Applied Thermal Engineering* 126, pp. 762-773.
Wang, X. and Dennis, M. 2017b. Phase Equilibrium and Formation Behavior of the $CO_2$–TBPB Semiclathrate Hydrate for Cold Storage Applications. *Journal of Chemical & Engineering Data* 62(3), pp. 1083-1093.
Wang, X. and Dennis, M. 2017c. Thermal energy harvest in the discharge of $CO_2$ semi-clathrate hydrate in an emulated cold storage system. *Applied Thermal Engineering* 124, pp. 725-733.
Waseem, M. S. and Alsaifi, N. M. 2018. Prediction of vapor-liquid-hydrate equilibrium conditions for single and mixed guest hydrates with the SAFT-VR Mie EOS. *The Journal of Chemical Thermodynamics* 117, pp. 223-235.
Xia, Z. et al. 2017. Hydrate-based Synchronously Capture of $CO_2$ and $H_2S$ for Clean $H_2$ with New Synergic Additives. *Energy Procedia* 142, pp. 3427-3432.
Xie, Y. et al. 2010. Experimental study on a small scale of gas hydrate cold storage apparatus. *Applied Energy* 87(11), pp. 3340-3346.
Xu, C.-G. et al. 2019. Insight into micro-mechanism of hydrate-based methane recovery and carbon dioxide capture from methane-carbon dioxide gas mixtures with thermal characterization. *Applied Energy* 239, pp. 57-69.
Yang, M. et al. 2013. Effects of additive mixtures (THF/SDS) on carbon dioxide hydrate formation and dissociation in porous media. *Chemical Engineering Science* 90, pp. 69-76.
Youssef, Z. et al. 2019. Management of vapor release in secondary refrigeration processes based on hydrates involving $CO_2$ as guest molecule. *International Journal of Refrigeration* 98, pp. 202-210.
Yu, Y.-S. et al. 2018. Crystal morphology-based kinetic study of carbon dioxide-hydrogen-tetra-n-butyl ammonium bromide hydrates formation in a static system. *Energy* 143, pp. 546-553.
Yue, G. et al. 2018. The combination of 1-octyl-3-methylimidazolium tetrafluorborate with TBAB or THF on $CO_2$ hydrate formation and $CH_4$ separation from biogas. *Chinese Journal of Chemical Engineering* 26(12), pp. 2495-2502.
Zhou, H. et al. 2015. Modelling and experimental validation of a fluidized bed based $CO_2$ hydrate cold storage system. *Applied energy* 158, pp. 433-445.
Zhou, S. et al. 2018. Investigation on the kinetics of carbon dioxide hydrate formation using flow loop testing. *Journal of Natural Gas Science and Engineering* 49, pp. 385-392.